

Experimental and molecular modeling study on the binary mixtures of [EMIM][BF₄] and [EMIM][TFSI] ionic liquids



José L. Trenzado^{a,*}, Ylenia Rodríguez^a, Alberto Gutiérrez^b, Alberto Cincotti^c, Santiago Aparicio^{b,*}

^aDepartamento de Física, Universidad de Las Palmas de Gran Canaria, 35017 Las Palmas G.C., Spain

^bDepartment of Chemistry, University of Burgos, 09001 Burgos, Spain

^cDepartment of Mechanical, Chemical and Materials Engineering, University of Cagliari, 09123 Cagliari, Italy

ARTICLE INFO

Article history:

Received 3 September 2020

Revised 4 March 2021

Accepted 31 March 2021

Available online 6 April 2021

Keywords:

Ionic liquids

Mixtures

Intermolecular forces

Thermodynamics

Molecular simulation

ABSTRACT

The properties of [EMIM][BF₄] + [EMIM][TFSI] double salt ionic liquid (DSIL) were studied as a function of mixtures composition and temperature. Experimental physicochemical properties combined with molecular simulation (quantum chemistry and classical molecular dynamics) were considered, thus providing a micro and macroscopic characterization of fluids' structuring, intermolecular forces and molecular aggregation. The results were analysed in thermodynamics terms considering deviations of ideality and mixing properties as well as from the solvation and interaction between the involved ionic liquids by the developed complex hydrogen bonding networks. Likewise, liquid [EMIM][BF₄] + [EMIM][TFSI] interfaces ($X_{[EMIM][BF_4]} = X_{[EMIM][TFSI]} = 0.5$) were also studied using molecular dynamics methods to examine the diffusion of [BF₄]⁻ and [TFSI]⁻ anions in the [EMIM][BF₄] + [EMIM][TFSI] liquid interface, and the mechanism of interface crossing. The results allow a multiscale characterization of the considered ionic liquid mixtures thus providing another way of designing IL-type solvents for specific applications, by choosing not only the ion identity but also the ion ratio.

© 2021 Elsevier B.V. All rights reserved.

1. Introduction

Ionic liquids (ILs) have attracted great attention because of their properties such as negligible vapor pressure [1], stability [2] or solvency power for different types of molecules [3,4], which combined with the variety of cation–anion combinations available (10¹⁸ possible mixed ILs [5]) show the possibility of considering ILs as designer solvents for process specific requirements [6]. Most of the available literature has considered so-called pure ILs, i.e. ILs formed by one type of cation plus one type of anion. However, a better-off structural diversity is achieved by mixing ILs, becoming an alternative “tool” to design tailor-made solvents for required technologies. Through the combination of more than one cation or anion in the mixture, a new concept of “double salt ILs” (DSILs) or blended ILs is obtained [7,8]. This definition allows a fuller consideration of the interactions generated between the mixture of ions and the presence of a new material. Combining ions in an IL may induce a preferential orientation of the ionic species and non-covalent interaction sites that would be markedly different from those possible in the single-component ILs [9,10]. The

remarkable advantage of using DSILs depends on a suitable anion–cation combination in order to accomplish more efficient electrochemical devices by designing task-specific IL mixtures. Although DSILs offer significant advantages over classical pure ILs as separation solvents, relevant studies are still scarce and a systematic DSIL selection method is thus highly desirable.

In a first systematic approach, IL mixtures may be studied considering a common cation and then analyse the effect of anion type. Canongia et al. [11] studied the deviation from ideality of IL mixtures (i.e. DSILs) containing [C₄MIm] as common cation, with anions such as PF₆⁻, BF₄⁻ or NTf₂⁻, using the measured excess molar volume. These systems showed small excess molar volumes, i.e. low deviations from ideality, being almost pressure and temperature independent. Stoppa et al. [12] considered [C₂MIm] as common cation and mixtures including BF₄⁻ and dicyanamide anions, also reporting almost linear behaviour with mixture composition for the studied mixtures and several thermophysical properties. Mixtures considering pyridinium – based cations with Tf₂N⁻ and dicyanamide anions were considered by Larriba et al. [13] reporting minor deviations from ideality for the reported mixtures. Pyrrolidinium – base cations and their mixtures involving NTf₂⁻ and dicyanamide anions were considered by Annat et al. [14] showing in all the cases simple mixing behaviour. The behaviour of systems including a common anion and the effect of cation type was also

* Corresponding authors.

E-mail addresses: jose.trenzado@ulpgc.es (J.L. Trenzado), sapar@ubu.es (S. Aparicio).

considered in the literature. The IL mixtures with common anions were considered by Navia et al. [15], considering BF_4^- anion and alkylimidazolium cations with variable chain length, and considering excess enthalpy and excess volume. These authors reported small deviations from ideality for the considered systems. These results were also confirmed through experimental measurements of viscosity, which show minor deviations from linear behaviour [16]. Mixtures with bis(trifluoromethylsulfonyl)imide as common anion and imidazolium, pyrrolidinium and piperazinium cations were studied by Oliveira et al. [17] considering surface tension and density measurements, thus reporting low deviations from linearity even for the largely different involved cations.

Therefore, the reported results for IL mixtures, both considering common anion or common cation, show minor deviations from linearity or small non-ideality behaviour with mixture composition. The IL mixtures studied in the literature have been reviewed [10], and although in most of the cases the deviations from ideality are minor, there are also systems containing large deviations [18]. Therefore, there is a need to clarify the molecular – level and nanoscopic roots on the behaviour of mixed ILs and their relationship with macroscopic properties. For this purpose, molecular simulation is a suitable approach to obtain the required information. The available studies on simulations for ILs mixtures were recently reviewed by Dhakal et al. [19], showing the prevailing role of the type of developed hydrogen bonds between the considered anions and cations and its role on the deviations from ideality. Nevertheless, the analysis of the local structure around ions is still very scarce and the information on local composition is still almost absent as well as the effect of developed intermolecular forces, specially hydrogen bonding.

Therefore, there is a lack of basic knowledge on the properties and molecular level structuring of DSILs mixtures, which need to be considered systematically to select the most suitable molecular combinations regarding the required properties for industrial applications. The use of DSILs have two notable advantages over two-ion ILs. Firstly, the number of DSILs resulting from the combinations of two-ion ILs is many orders of magnitude larger, so they significantly extend the solvent selection space [20]. Secondly, DSILs offer an easy approach to tune solvent properties. For example, Pinto et al. observed that the viscosity of the “mixture” of $[\text{C}_2\text{MIm}][\text{NTf}_2]$ and $[\text{C}_4\text{Elm}][\text{EtSO}_4]$ varies from 32.6 to 255.2 mPa·S with the molar fraction of $[\text{C}_4\text{Elm}][\text{EtSO}_4]$ increasing from 0 to 1 [21]; Lei et al. found that the solubility of CO_2 in the “mixture” of $[\text{C}_8\text{MIm}][\text{NTf}_2]$ and $[\text{C}_n\text{MIm}][\text{BF}_4]$ ($n = 2, 4$) can be adjusted by different IL compositions [22]. Therefore, DSILs open new horizons for the identification of suitable solvents for separation processes. For this, the study DSILs mixtures requires a systematic approach, considering the large number of possible combinations and the mixture composition effects. The main objectives should be, on the one hand, to analyse the intermolecular forces (cation–anion dimers, cation–anion–anion trimer and cation–anion–cation–anion tetramer) and microscopic behaviour [23] as a function of the mixed components and composition and, on the other hand, to infer their effects and relationships with macroscopic physico-chemical properties [24] to develop predictive models. The microscopic level information on DSILs systems can be inferred from molecular modelling studies, for which the combined use of density functional theory (DFT) and classical molecular dynamics simulations (MD) could be suitable. In the same way, the macroscopic level vision of DSILs can be inferred from the experimental determination of selected thermophysical properties, with relevance for process design purposes [25]. The combination of both experimental and molecular modelling studies leads to the required micro and macroscopic characterization. The studies as function of mixtures composition, pressure and temperature, allow to

characterize the intermolecular forces, deviations from ideality and structural changes upon mixing

Our research group has been developing a systematic theoretical and experimental research for different types of ILs with, for example, molecular solvents (MSs), where starting from ILs based on alkylimidazolium cations and different types of anions the mixtures with relevant MSs such as water, alcohols, acetone, acetonitrile, dimethylformamide, ethylene glycol or dimethylsulfoxide have been considered [26–30]. However, as previously mentioned, in the case of DSILs there is still much to study. Therefore, in this work a study of 1-ethyl-3-methylimidazolium coupled with tetrafluoroborate and bistriflimide ($[\text{EMIM}][\text{BF}_4]$ and $[\text{EMIM}][\text{TFSI}]$) ILs and their binary mixtures containing a common cation (DSILs) has been reported in the full composition range as a function of temperature. For these systems, microstructuring and characterization of intermolecular forces is not available in the literature. Therefore, the reported results allow to infer the mechanism of molecular interaction between $[\text{EMIM}][\text{BF}_4]$ and $[\text{EMIM}][\text{TFSI}]$ ILs and their binary constituent mixtures with $[\text{EMIM}]^+$ as common cation. Likewise, MD simulations on $[\text{EMIM}][\text{BF}_4] + [\text{EMIM}][\text{TFSI}]$ interfaces ($X_{[\text{EMIM}][\text{BF}_4]} = X_{[\text{EMIM}][\text{TFSI}]} = 0.5$) were carried out, inferring the diffusion of $[\text{BF}_4]^-$ and $[\text{TFSI}]^-$ anions across the interface and the behaviour at $[\text{EMIM}][\text{BF}_4] + [\text{EMIM}][\text{TFSI}]$ liquid interfaces. The selection of these ILs was done considering that the available literature have showed minor deviations from ideality for alkylimidazolium – based cations but the nanoscopic behaviour of these systems is not clarified, neither in the evolution of excess and mixing properties nor in the changes in intermolecular forces upon mixing and the local composition effects. The main novelty of this work stands on the combination of highly accurate thermophysical studies with molecular modelling, as a function of composition and temperature, which may led to the required insights into the mixtures properties.

2. Methods

2.1. Materials

The chemicals used for the experimental study, reported in Table S1 (Supplementary Information), were obtained from commercial suppliers and were used without additional purification. Pure ILs were degassed by ultrasound, handled under inert atmosphere and water content measured. The properties of pure ILs were measured as a function of temperature (283.15 to 313.15 K range) and compared with literature, Table S2 (Supplementary Information), showing minor differences, which can be attributed to water content and different origin of the samples [31], but discards the presence of relevant impurities [32]. The mixture samples ($x [\text{EMIM}][\text{BF}_4] + (1-x) [\text{EMIM}][\text{TFSI}]$, where x stands for mole fraction) were prepared in the full composition range by weighing (Mettler AE240 balance, ± 0.01 mg) to ± 0.00004 estimated mole fraction uncertainty.

2.2. Thermophysical properties

Density (ρ) and kinematic viscosity (ν) were measured in the 283.15 to 313.15 K range, in 5 K steps at atmospheric pressure conditions. Kinematic viscosity data were converted to dynamic viscosity (η) data by using experimental density data and used along the work, eq. (1).

$$\eta = \nu \times \rho \quad (1)$$

Density was measured with a vibrating tube densitometer (Anton Paar DMA5000) with cell temperature controlled with Peltier elements and measured to ± 0.01 K. The densitometer was

calibrated with water (Panreac Hiperpur-plus) and n-heptane (Fluka > 99.5%) as reference fluids [33,34], thus leading to $\pm 0.00002 \text{ g cm}^{-3}$ uncertainty. Kinematic viscosity was measured using capillary viscometry (Schott-Geräte AVS350), with the cell temperature measured with $\pm 0.01 \text{ K}$ uncertainty. Viscometer calibration was carried out with suitable reference oils, thus leading to 0.4% overall uncertainty.

Excess and mixing properties derived properties from experimental data were calculated using well-known thermodynamics equations [35] according to the relationships reported in the [Supplementary Information](#). Density data allowed the calculation of excess molar volume, V^E , as well as the partial molar volumes of each compound in a mixture, \bar{V}_i , the corresponding excess value, \bar{V}_i^E , and the value at infinite dilution, $\bar{V}_i^{E,\infty}$. Likewise, isobaric expansivity, α_p , was inferred from linear fits of ρ vs temperature ($R^2 \geq 0.99999$) together with the excess property, α_p^E . Regarding viscosity, as it is not possible to define an ideal reference term, the so-called mixing viscosity, $\Delta\eta$, was calculated.

2.3. Molecular modelling

Density Functional Theory Calculations. Initial structures for all the considered molecules and molecular clusters were built with Avogadro program [36] and optimized with ORCA software [37]. DFT calculations were carried out using B3LYP functional [38,39], coupled with van der Waals semiempirical contribution from DFT-D3 method by Grimme [40], and 6-311++G** basis set. The interaction energy (ΔE) for all the considered structures was calculated, considering Basis Set Superposition Error (BSSE) corrected by using counterpoise method [41].

The quantum theory of atoms-in-molecules (Bader's AIM theory [42]) was applied for the topological analysis of intermolecular forces, with particular attention to hydrogen bonding, using the Multiwfn program [43]. AIM analysis characterizes interaction regions by so-called bond critical points (BCP, (3,-1) type according to Bader's terminology) and ring critical points (RCP, (3,+1) type) and the corresponding values of electron density, ρ , and Laplacian of electron density, $\nabla^2\rho$ [44]. The analysis of the inferred critical points may be related with the strength and nature of the interactions [45,46] which was complemented by the use of the Reduced Density Gradient analysis (RDG) [47].

Classical Molecular Dynamics Simulations. MD simulations were carried out with MDynaMix v.5.2 [48] for the forcefield parameterizations reported in Table S3 ([Supplementary Information](#)) for the systems and conditions included in [Figures S1 and S2](#) and Table S4 ([Supplementary Information](#)). MD simulations were carried out for [EMIM][BF₄] with [EMIM][TFSI] mixtures in the full composition range. For the three studied ions, force field parameters were extracted from SwissParam database [49], which considers a Merck Molecular Force Field [50], with the exception of atomic charges which were calculated from DFT (B3LYP-D3/6-311++G**) results for optimized structures of isolated monomers using ChelpG approach [51]. The [EMIM][BF₄] + [EMIM][TFSI] solutions studied using MD, Table S4 ([Supporting Information](#)), consider *i*) the full composition range to infer different solvation conditions and *ii*) the diffusion of [BF₄]⁻ and [TFSI]⁻ anions at [EMIM][BF₄] + [EMIM][TFSI] liquid interface. Initial simulation boxes for each solution composition were built with PACKMOL [52] program for densities 20% lower than those of the corresponding pure ILs, [Figures S1 and S2](#) ([Supplementary Information](#)). A single initial simulation box was prepared for each mixture composition, thus, to avoid dependence with the considered initial configuration heating and quenching steps were developed before production runs. Periodic boundary conditions were applied in the three spatial directions. These pre-equilibration runs were developed as follows: *i*)

heating up to 500 K, *ii*) NPT simulations at 500 K and 1 bar for 5 ns, *iii*) quenching to 298 K, *iv*) NPT simulations at 298 K and 1 bar for 5 ns. This heating and quenching procedure was repeated three times per mixture composition with the last configuration used for final MD simulations. The moderate viscosity of the considered ILs (34.69 and 58.46 mPa s for [EMIM][BF₄] and [EMIM][TFSI], respectively, Table S2 in the [Supplementary Information](#)) assures negligible dependence of the trajectories with regard to the initial configuration using this procedure. The final simulations, starting from the final one from heating – quenching cycles, were carried out in the NPT ensemble at 298 K and 1 bar considering a 10 ns equilibration step followed by 20 ns production run. For the simulation of IL mixture at vacuum interface, 40 ns of production was launched. The control of pressure and temperature was done using the Nose–Hoover method. Electrostatic interactions were treated with the Ewald method [53] (15 Å for cut-off radius). Lennard-Jones cross terms were calculated using Lorentz–Berthelot mixing rules. The Tuckerman–Berne double time step algorithm [54] (1 and 0.1 fs for long and short-time steps) was applied for the equations of motion. Data analysis and visualization was done with MDynaMix – TRANAL [39], VMD [55] and TRAVIS [56] programs (See [Fig. 1](#)).

3. Results and discussion

3.1. Experimental study

Experimental density and viscosity data for the studied IL mixtures are reported in Table S5 ([Supplementary Information](#)) as well as the derived V^E and $\Delta\eta$. Likewise, density and viscosity data as a function of composition were fitted to polynomials, whereas V^E and $\Delta\eta$ were fitted to Redlich–Kister polynomials, with all the fitting coefficients being reported in Table S6 ([Supplementary Information](#)). All the properties are reported in the 283.15 to 313.15 K range. Results in [Fig. 2a](#) show ρ evolution with mixture composition with ρ vs mole fraction showing a largely non-ideal behavior, with ρ being larger than the linear evolution in the whole composition range. This densification effect upon mixing is maintained in the studied temperature range, thus pointing to strong heteroassociations upon mixing and confirming that the mixture of these two

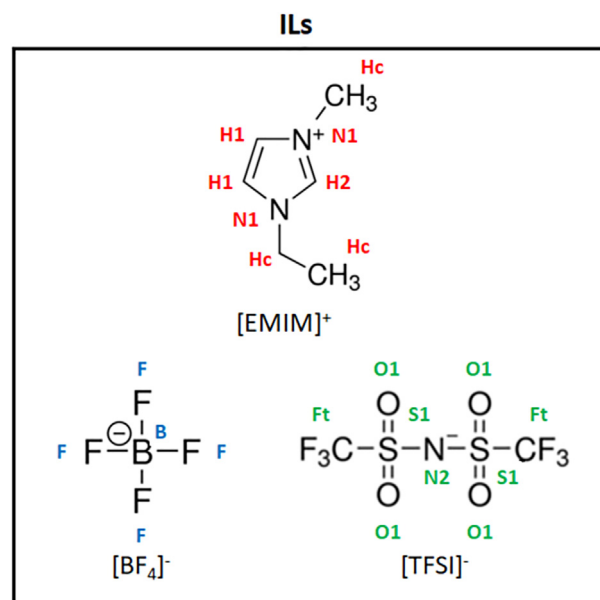


Fig. 1. Molecular structures for ILS studied in this work.

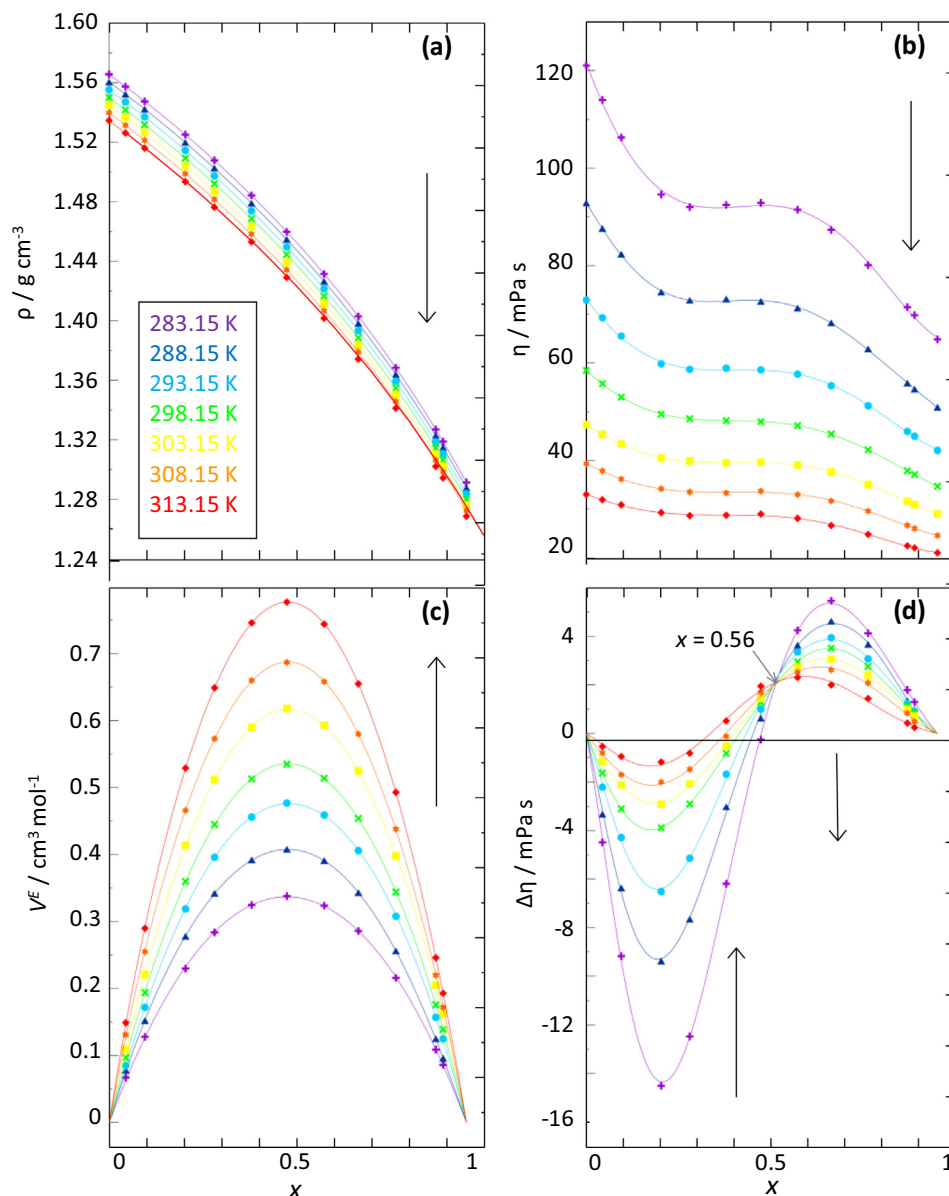


Fig. 2. Experimental thermophysical properties for x [EMIM][BF₄] + (1- x) [EMIM][TFSI], x stands for mole fraction, mixtures as a function of temperature. ρ , density, η , dynamic viscosity, V^E , excess molar volume and $\Delta\eta$, mixing viscosity. Black arrows indicate increasing temperature for guiding purposes. Gray arrow in panel d indicates the composition for the intersection point.

ILs, although containing a common cation leads to complex effects beyond the simple ion replacement. It should be remarked that although the mixture [EMIM][BF₄] + [EMIM][TFSI] could be considered as a simple IL with one type of cation ([EMIM]) and two different anions ([BF₄] and [TFSI]), i.e. a double salt IL, the presence of two different types of anions leads to complex intermolecular forces. This is confirmed by the composition evolution of η , Fig. 2b, which is largely non-linear with different behavior as a function of x . The viscosity of neat [EMIM][BF₄] is lower than for [EMIM][TFSI], therefore ongoing from neat [EMIM][TFSI] to neat [EMIM][BF₄], i.e. the replacement of [TFSI] anions per [BF₄] ones is accompanied by a decrease in η , but this evolution is not a simple composition effect as showed in Fig. 2b. Three well-defined regions are inferred for the evolution of η vs mole fraction ([BF₄] content): *i*) x in 0 to 0.2 range, *ii*) x in 0.2 to 0.6 range and *iii*) x in 0.6 to 1.0 range. Regions *i* and *iii* are characterized by a decrease in viscosity with increasing [BF₄], thus pointing to an

anion replacement interaction mechanism, but region *iii* surprisingly shows constant viscosity. The behavior of region *iii* in terms of viscosity show the development of new intermolecular forces which are not present in the neat ILs and an interaction mechanism different to the simple anion replacement around the central cations. These new intermolecular forces should be strong enough to maintain the high viscosity instead of the decreasing effect because of the presence of [BF₄] anion. Although previous literature studies have claimed almost negligible deviations from ideality for alkylimidazolium based ILs [11,12,15,16,17], results in Fig. 2c and 2d show that mixtures studied in this work are far from an ideal system. This non-ideal behavior indicates the presence of intermolecular effects not present in the neat ILs which determine the properties of the mixed, DSILs. The V^E are remarkably large in the whole composition and temperature range with maxima at equimolar mixture compositions. The behavior of $\Delta\eta$ is extremely complex, with negative values below for [TFSI] rich systems and

positive ones for [BF₄] rich mixtures, thus confirming the effect of intermolecular forces on mixtures behavior.

The volumetric properties allowed the calculation of \bar{V}_i^E , Fig. 3a and 3b, and the values at infinite dilution, $\bar{V}_i^{E,\infty}$, Fig. 3c. The behaviour of \bar{V}_i^E is very symmetric for both components, with similar positive values in the whole composition range and increasing with temperature. These values of the excess partial molar volumes confirm the strength of intermolecular forces. Likewise, the large values of $\bar{V}_i^{E,\infty}$ show the disrupting effect of one type of anion on the structuring of the other one, thus leading to new intermolecular interactions upon anion replacements. The values of α_p and α_p^E reported in Fig. 4 agree with high non-ideality inferred from the other thermophysical properties. The α_p vs mole fraction evolution, Fig. 4a, is largely non-linear, evolving through maxima around equimolar composition. Therefore, for [TFSI] – rich mixtures the addition of [BF₄] leads to a more compressible fluid, i.e. [BF₄] disrupting effect, which agrees with the behaviour of viscosity, but after this, the increasing [BF₄] content decreases fluids' compressibility, therefore fluids' rearrangements are confirmed again. Nevertheless, α_p^E , Fig. 4b, are positive in the whole composition range, thus confirming the disrupting effect because of the simultaneous presence of both types of anions.

The information obtained from the reported thermophysical properties may be extended through the use of suitable models, which allow to connect the macro with the microscopic information. Therefore, the Prigogine-Flory-Patterson (PFP) [57] has been considered for the prediction of V^E . PFP model allows to infer the

different contributions to V^E , thus dividing it as the sum of interactional, free volume and P^* contributions. The excellent performance of PFP model for describing V^E with a single model parameter is confirmed in Fig. 5a for all the studied temperatures. The interactional contribution to total V^E allows to analyse the intermolecular interactions effects, being quantified through the χ_{12} interaction parameter. This interactional contribution, Fig. 5b, is positive in the whole composition range and remarkably larger than the other two ones, Fig. 5c and 5d, being the main contribution to the total V^E , thus confirming the role of the newly developed intermolecular forces on the behaviour of V^E , being on the roots of the large non-ideality of the studied mixtures. Likewise, the linear evolution of χ_{12} with increasing temperature, Fig. 6, confirms that the role of intermolecular forces is maintained in the whole temperature range. The free volume and P^* contributions to the total V^E are negative but remarkably smaller, in absolute value, than the interactional contribution. Thus, packing effects because of the different sizes and shapes of [BF₄] and [TFSI] anions do not have a remarkable effect on V^E being mainly produced because of the newly developed intermolecular forces.

The modelling of viscosity is largely complex considering the complex composition evolution as reported in Fig. 2b. The temperature evolution of viscosity can not be described with a simple Arrhenius equation and thus Vogel – Fulcher – Tamman (VFT) model was considered in the studied temperature range, with the model parameters reported in Fig. 7. The three VFT parameters follow a non-linear evolution with mixture composition, in agreement with behaviour reported in Fig. 2b, with larger differences

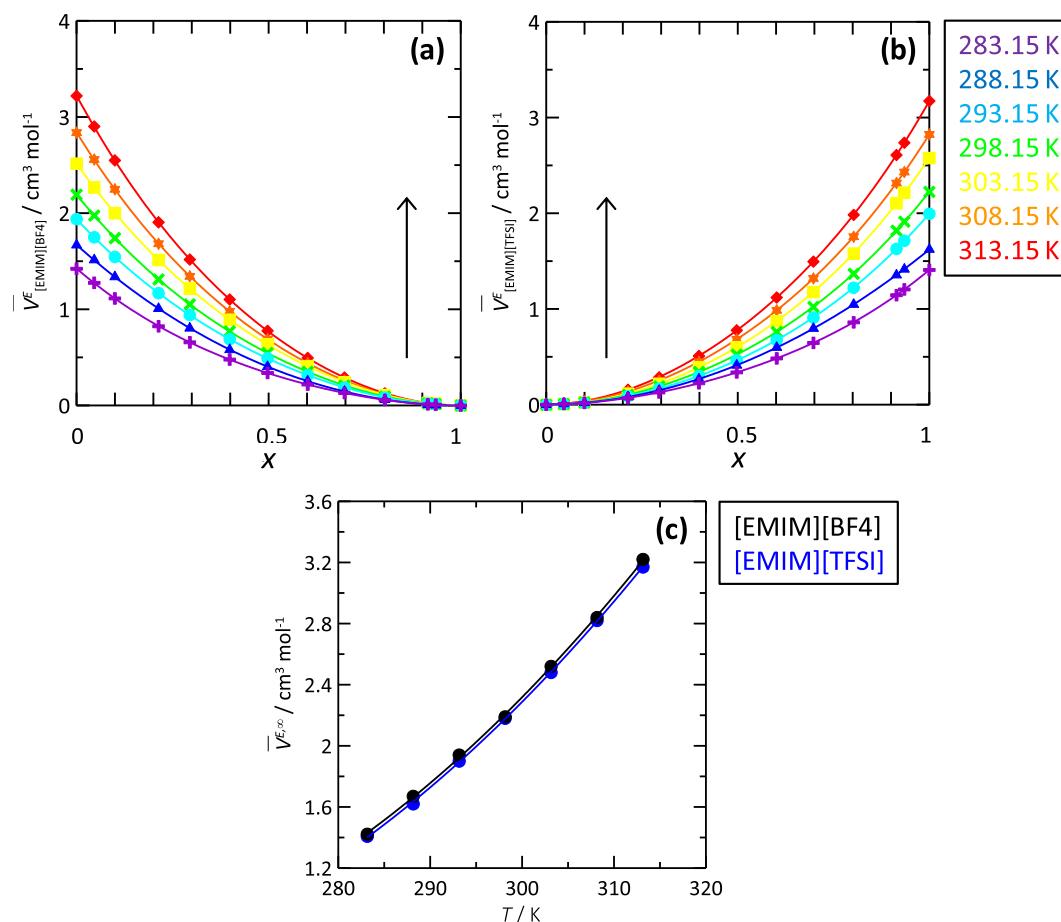


Fig. 3. (a,b) Excess partial molar volume, \bar{V}_i^E , and (c) values at infinite dilution, $\bar{V}_i^{E,\infty}$, for x [EMIM][BF₄] + (1-x) [EMIM][TFSI], x stands for mole fraction, mixtures as a function of temperature. Black arrows indicate increasing temperature for guiding purposes. Values in panels a and b show V^E for [EMIM][BF₄] and [EMIM][TFSI], respectively.

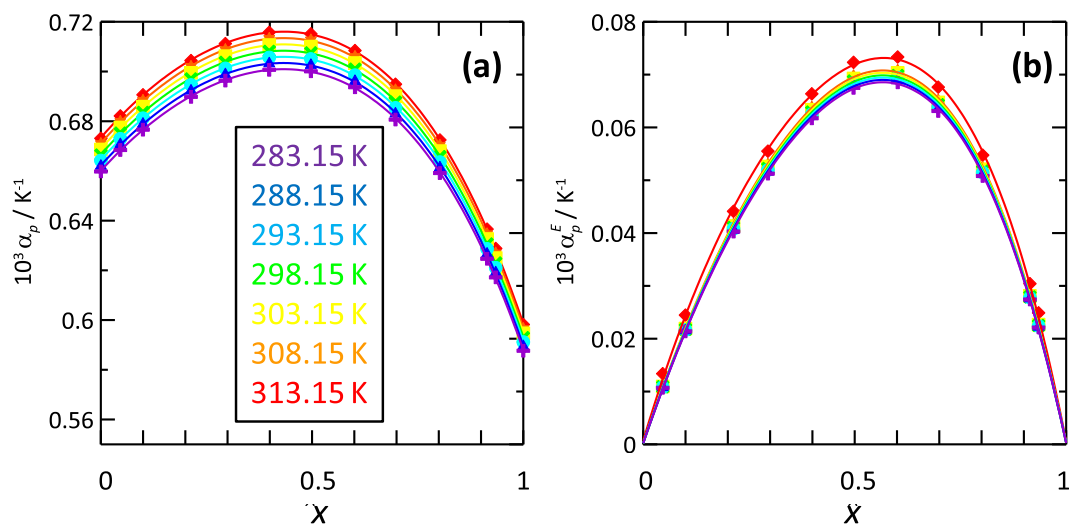


Fig. 4. (a) Isobaric thermal expansion coefficient, and (b) excess isobaric thermal expansion coefficient, for x [EMIM][BF₄] + (1-x) [EMIM][TFSI], x stands for mole fraction, mixtures as a function of temperature.

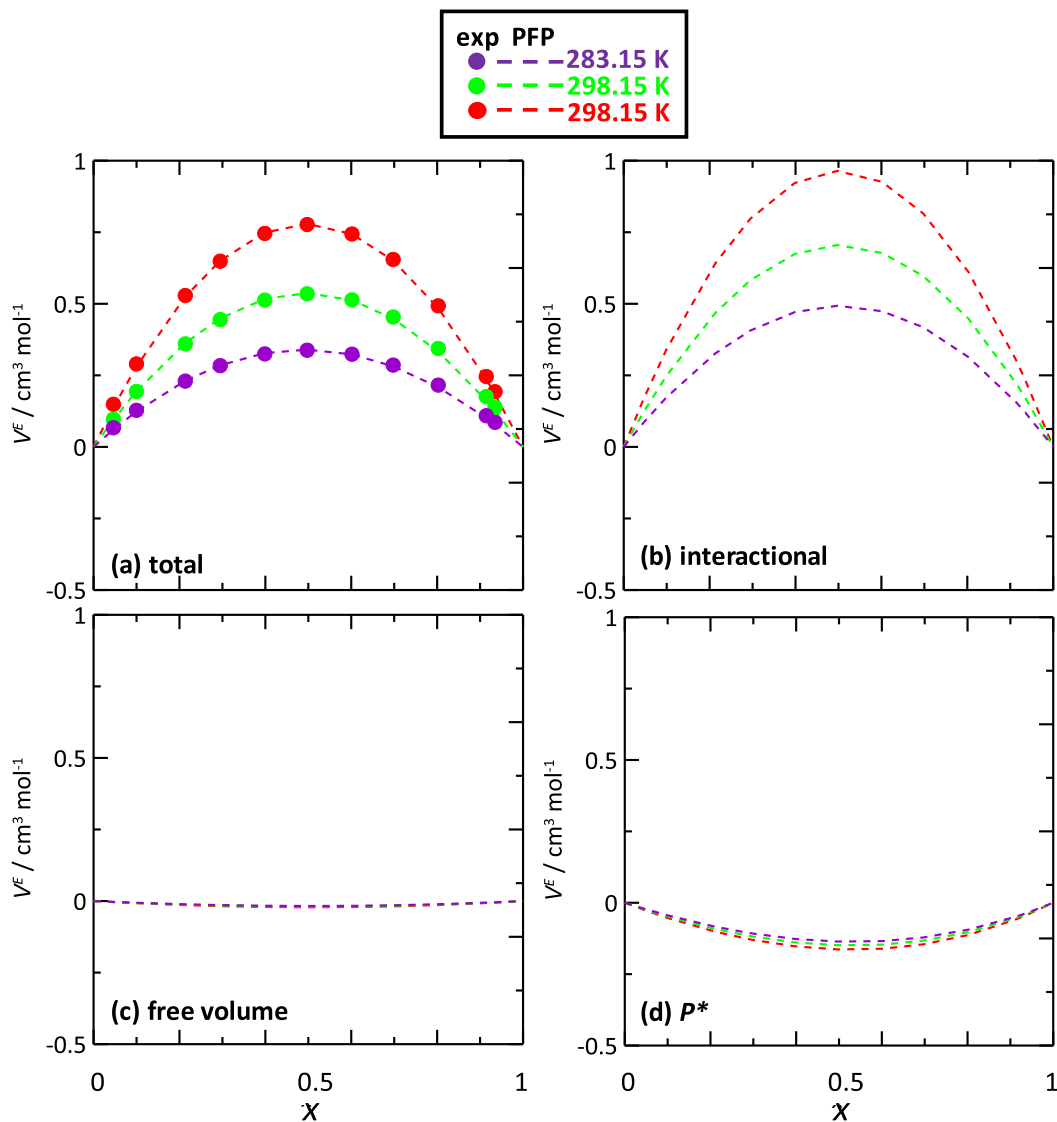


Fig. 5. Comparison of experimental, exp, and Prigogine-Flory-Patterson, PFP, excess molar volume, V^E , x [EMIM][BF₄] + (1-x) [EMIM][TFSI], x stand for mole fraction, mixtures as a function of temperature. Results in panels b to d show interactional, free volume and P* PFP contributions to the total V^E .

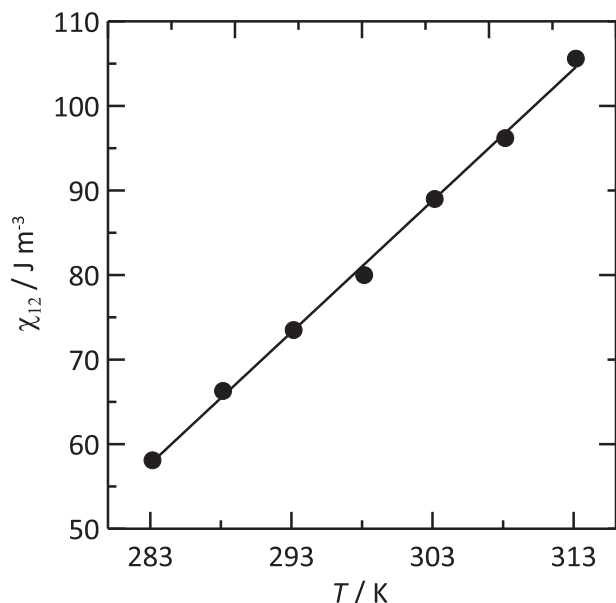


Fig. 6. χ_{12} parameter from the fitting of excess molar volume for x [EMIM][BF₄] + (1-x) [EMIM][TFSI], x stand for mole fraction, mixtures as a function of temperature.

for the central composition region around equimolar mixtures. The T_0 parameter, which is close to the glass transition temperature, shows maxima for equimolar mixtures and minima both in [TFSI] and [BF₄] – rich mixtures, thus confirming large structural changes upon anion composition evolution because of the modification of intermolecular forces. Therefore, the reported thermophysical properties show complex behaviour for the studied IL mixtures beyond a simple effect of anion replacement, which can be related to changes in the nature and extension of intermolecular forces. These effects are analysed at the nanoscopic level using molecular modelling tools in sections 3.2 and 3.3.

3.2. DFT modelling of [EMIM][BF₄], [EMIM][TFSI], [EMIM][BF₄] + [TFSI] and [EMIM][BF₄] + [EMIM][TFSI] interactions

In the present study, we analyse the mechanism(s) of [EMIM][BF₄], [EMIM][TFSI], [EMIM][BF₄] + [TFSI] and [EMIM][BF₄] + [EMIM][TFSI] short-range interactions, hydrogen bonding. Different interaction sites were considered, and the structures were geometrically optimized, Fig. 8. The strength of interactions between dimers, trimer and tetramer at different possible interaction sites was quantified through counterpoise corrected binding energies, E_{int} , Table 1. The reported E_{int} are larger (in absolute value) for tetramer than for trimer and dimer, and larger for TFSI dimer than for BF₄ dimer. The mechanism of dimers, trimer and tetramer interactions is depicted in Fig. 8. The presence of hydrogen bond accepting sites (F atoms in [BF₄]⁻ anion and O/F atoms in [TFSI]⁻ anion) and donor sites (H atoms in [EMIM]⁺ cation) in ILs leads to the possibility of developing anion-cation hydrogen bonding. Nevertheless, it is well-known that for the considered [EMIM][BF₄] anion-cation hydrogen bonding between the F atoms of the anion and the CH (2) (carbon atom between both N atoms in imidazolium ring) site in imidazolium is developed [58]. In the case of [EMIM][TFSI] IL, it is also well-known that most of the hydrogen bonds are formed with oxygen atoms as hydrogen acceptors [59] (specifically, the strongest hydrogen bonds are produced between the O(1) atoms of the anion and the CH(2) site in imidazolium). Thus, in the case of the [EMIM][BF₄] + [TFSI] trimer, [BF₄]⁻/[TFSI]⁻ anions may compete for this interaction site and also they may develop hydrogen bonding through the CH(1) (the other two CH sites in imidazolium

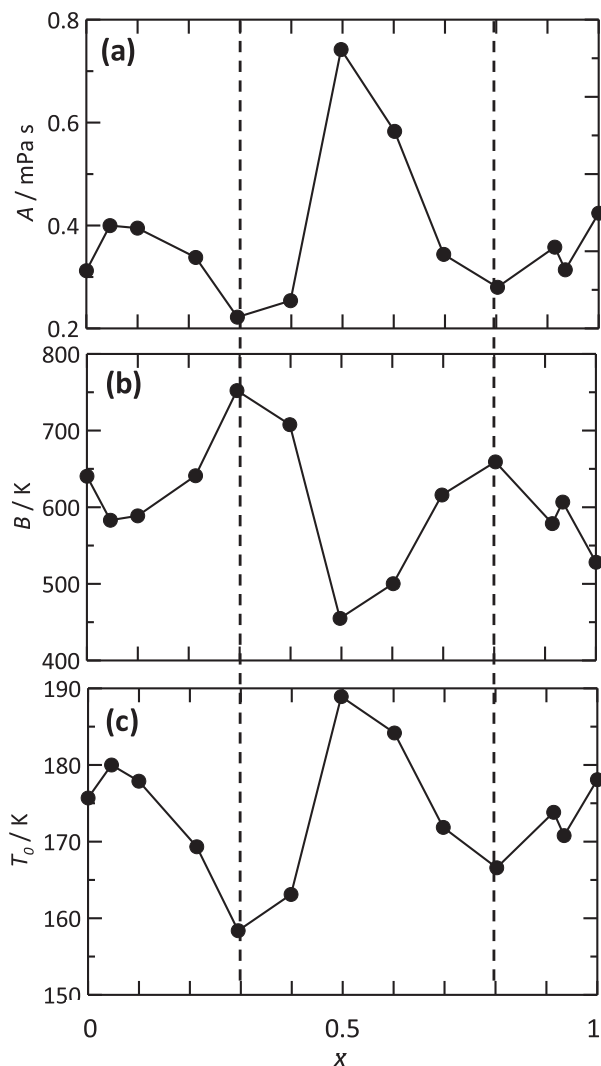


Fig. 7. Fitting parameters of VFT equation for dynamic viscosity for x [EMIM][BF₄] + (1-x) [EMIM][TFSI], x stands for mole fraction, mixtures in the 283.15 to 313.15 K temperature range.

ring) sites in imidazolium ring. For the [EMIM][BF₄] + [EMIM][TFSI] tetramer, it is observed that the [TFSI]⁻ anion interacts through its O(1) atoms with the two [EMIM]⁺ groups, while the [BF₄]⁻ anion only interacts through its F atoms with one of the [EMIM]⁺ groups. The interaction between [EMIM][BF₄] and [TFSI]/[EMIM][TFSI] does not lead neither to large charge transfer toward [TFSI]/[EMIM][TFSI] nor through relevant changes in anion and cation total charges, Fig. 8, thus interaction being van der Waals and hydrogen bonding types.

The dimers, trimer and tetramer interactions were also analysed using the Bader's Atoms in a Molecule (AIM) theory, using the optimized geometries in the Multiwfn code. Hydrogen bonding is topologically analysed in the AIM framework considering the electron density and the formation of bond critical points (BCPs, type (3,-1) in AIMs naming) and additional features like ring critical points (RCPs, type (3,+1)) along the line joining hydrogen donor and acceptor sites. The properties of these critical points (CPs) are quantified with the values of electron density, ρ , and Laplacian of electron density, $\nabla^2\rho$. Likewise, the AIM topological characterization for hydrogen bonding indicates that ρ and $\nabla^2\rho$ must be in the 0.002 to 0.04 a.u. and 0.020 to 0.139 a.u. ranges, respectively, with larger values indicating stronger hydrogen bonds [60].

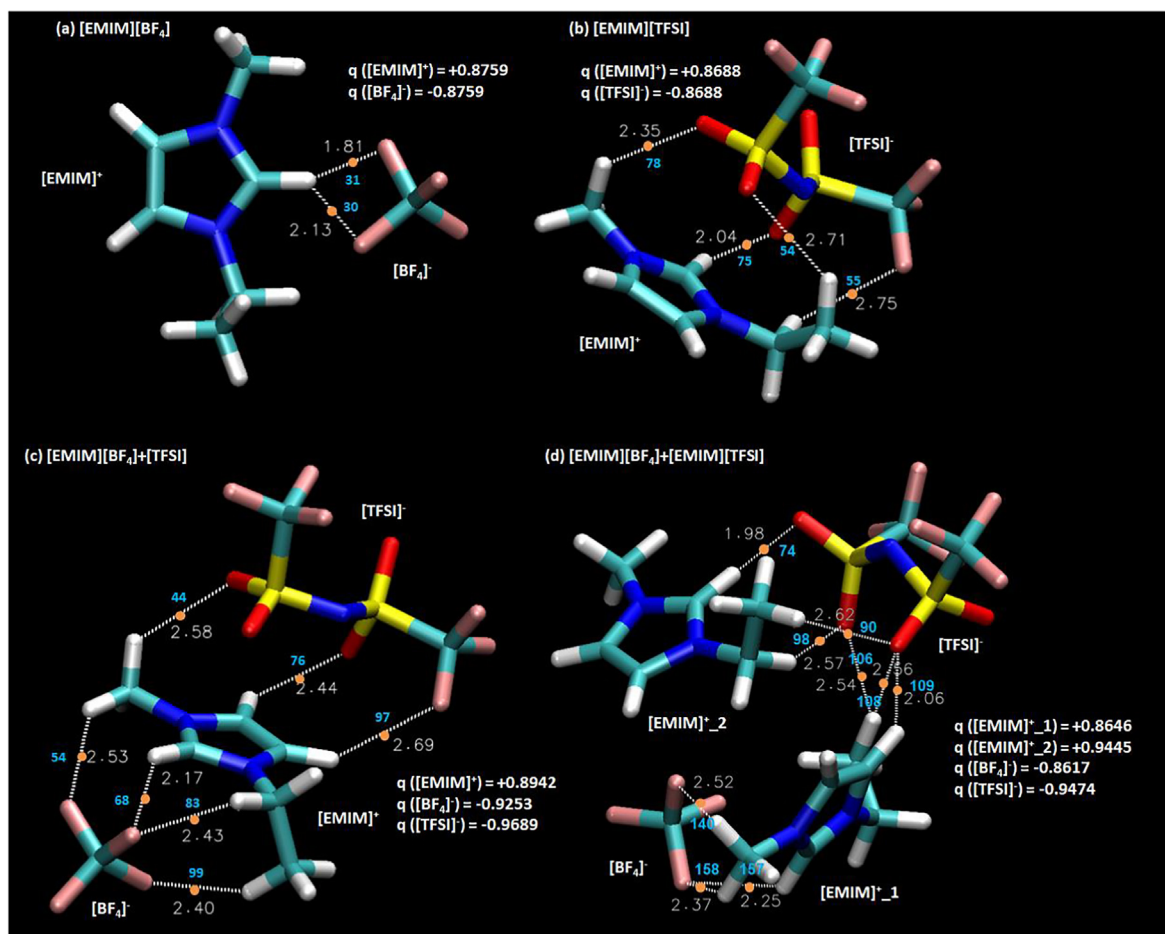


Fig. 8. Atom in molecule (AIM) analysis of interactions, bond critical points (BCPs) and CHELPG charges for (a) [EMIM][BF₄], (b) [EMIM][TFSI], (c) [EMIM][BF₄] + [TFSI], (d) [EMIM][BF₄] + [EMIM][TFSI]. Electron density (ρ) and Laplacian of electron density ($\nabla^2\rho$) for BCPs are reported separately in Table 2.

Table 1

Properties for [EMIM]⁺[BF₄]⁻, [EMIM]⁺[TFSI]⁻, [EMIM]⁺[BF₄]⁻ + [TFSI]⁻ and [EMIM]⁺[BF₄]⁻ + [EMIM]⁺[TFSI]⁻ systems that are calculated at a B3LYP-D3/6-311++G** theory level. Counterpoise corrected interaction energy, (E_{int}); HOMO (E_{HOMO}) and LUMO (E_{LUMO}) energies; HOMO-LUMO energy gap (ΔE_G).

structure	E_{int} / eV	E_{HOMO} / eV	E_{LUMO} / eV	ΔE_G / eV
[EMIM] ⁺ [BF ₄] ⁻	-3.62	-8.31	-1.48	-6.83
[EMIM] ⁺ [TFSI] ⁻	-3.64	-7.52	-1.48	-6.04
[EMIM] ⁺ [BF ₄] ⁻ + [TFSI] ⁻	-4.87	-4.89	1.74	-6.63
[EMIM] ⁺ [BF ₄] ⁻ + [EMIM] ⁺ [TFSI] ⁻	-8.18	-7.45	-1.27	-6.18

Although dimers, trimer and tetramer interactions are characterized by many CPs, as inferred from the mechanism(s) of interaction in Fig. 8, the most relevant, i.e. stronger, BCPs are reported in Table 2. Results in Table 2 summarize the interactions leading to the stronger BCPs, i.e. CPs with larger ρ and $\nabla^2\rho$, and thus possible hydrogen bond interactions. In all cases, weak hydrogen bonds are formed between [EMIM][BF₄], [EMIM][TFSI], [EMIM][BF₄] + [TFSI] and [EMIM][BF₄] + [EMIM][TFSI]. It should be remarkable that in the case of [EMIM][BF₄] + [TFSI] trimer, larger values are inferred for interaction between the F atom of [BF₄]⁻ and the CH(2) carbon atom between both N atoms in [EMIM]⁺ (BCP 68), and also for interaction between the O(1) atom of [TFSI]⁻ and the CH(1) site in [EMIM]⁺ (BCP 76). In the case of [EMIM][BF₄] + [EMIM][TFSI] tetramer, larger values are inferred for interaction between the F atom of [BF₄]⁻ and the CH(2) carbon atom between both N atoms in [EMIM]⁺ (BCP 157), and also for interaction between the O(1) atom of [TFSI]⁻ and the CH(2) site in [EMIM]⁺ (BCP 74). The large interaction energy reported in Table 1 seems to be justified not by the

development of single very strong hydrogen bonds but because of the dimers, trimer and tetramer abilities for developing a large number of interactions, as reported in Fig. 8 and confirmed by the large number of BCPs.

Additional analysis of quantum chemistry results for dimers, trimer and tetramer can be done using the Noncovalent interaction (NCI) analysis [61] according to the Reduced Density Gradient (RDG) surfaces. The RDG scatter plots are reported in Fig. 9 showing that hydrogen bonding characteristics regions are inferred, blue spots. In all cases, these regions are narrow and closer to the lower limit of hydrogen bonding region, thus confirming the minor extension of hydrogen bonding. Additionally, RDG regions corresponding to van der Waals-like interactions, green spots, are inferred, which show that these type of weaker interactions should have a remarkable contribution to the large interaction energies reported in Table 1. This mechanism of interaction is confirmed with the RDG isosurfaces reported in Figure S3 (Supporting Information), in which the green spots for all the interaction sites point

Table 2

Atoms-in-a-molecule analysis of the reported [EMIM⁺][BF₄], [EMIM⁺][TFSI], [EMIM⁺][BF₄] + [TFSI⁻] and [EMIM⁺][BF₄] + [EMIM⁺][TFSI⁻] systems calculated at the B3LYP-D3/6-311++C** level. Bond critical points (BCP, (3, -1)) are provided in the table. Electron density (ρ) and Laplacian of electron density ($\nabla^2\rho$) at the corresponding BCP are provided as a guide for AIM and RDG figure analysis. The most remarkable interactions are reported in bold.

structure	BCP(s)	ρ / a.u.	$\nabla^2\rho$ / a.u.	Interaction sites
[EMIM ⁺][BF ₄]	30	0.0174	0.0717	[EMIM ⁺](H2) ··· (F)[BF ₄]
	31	0.0313	0.1229	[EMIM⁺](H2) ··· (F)[BF₄]
[EMIM ⁺][TFSI ⁻]	54	0.0063	0.0212	[EMIM ⁺](Hc) ··· (O1)[TFSI ⁻]
	55	0.0042	0.0180	[EMIM ⁺](Hc) ··· (Ft)[TFSI ⁻]
	75	0.0221	0.0809	[EMIM⁺](H2) ··· (O1)[TFSI⁻]
	78	0.0125	0.0442	[EMIM ⁺](Hc) ··· (O1)[TFSI ⁻]
	83	0.0093	0.0339	[EMIM ⁺](Hc) ··· (F)[BF ₄]
[EMIM ⁺][BF ₄] + [TFSI ⁻]	44	0.0079	0.0262	[EMIM ⁺](Hc) ··· (F)[BF ₄]
	54	0.0070	0.0262	[EMIM ⁺](Hc) ··· (O1)[TFSI ⁻]
	68	0.0155	0.0604	[EMIM⁺](H2) ··· (F)[BF₄]
	76	0.0109	0.0406	[EMIM⁺](H1) ··· (O1)[TFSI⁻]
	83	0.0093	0.0339	[EMIM ⁺](Hc) ··· (F)[BF ₄]
	97	0.0044	0.0179	[EMIM ⁺](H1) ··· (Ft)[TFSI ⁻]
	99	0.0093	0.0325	[EMIM ⁺](Hc) ··· (F)[BF ₄]
	74	0.0242	0.0881	[EMIM⁺](H2) ··· (O1)[TFSI⁻]
	90	0.0077	0.0270	[EMIM ⁺](Hc) ··· (O1)[TFSI ⁻]
	98	0.0083	0.0248	[EMIM ⁺](Hc) ··· (O1)[TFSI ⁻]
[EMIM ⁺][BF ₄] + [EMIM ⁺][TFSI ⁻]	106	0.0086	0.0308	[EMIM ⁺](Hc) ··· (O1)[TFSI ⁻]
	108	0.0083	0.0251	[EMIM ⁺](Hc) ··· (O1)[TFSI ⁻]
	109	0.0191	0.0786	[EMIM ⁺](H1) ··· (O1)[TFSI ⁻]
	140	0.0088	0.0366	[EMIM ⁺](Hc) ··· (F)[BF ₄]
	157	0.0142	0.0550	[EMIM⁺](H2) ··· (F)[BF₄]
	158	0.0108	0.0397	[EMIM ⁺](Hc) ··· (F)[BF ₄]

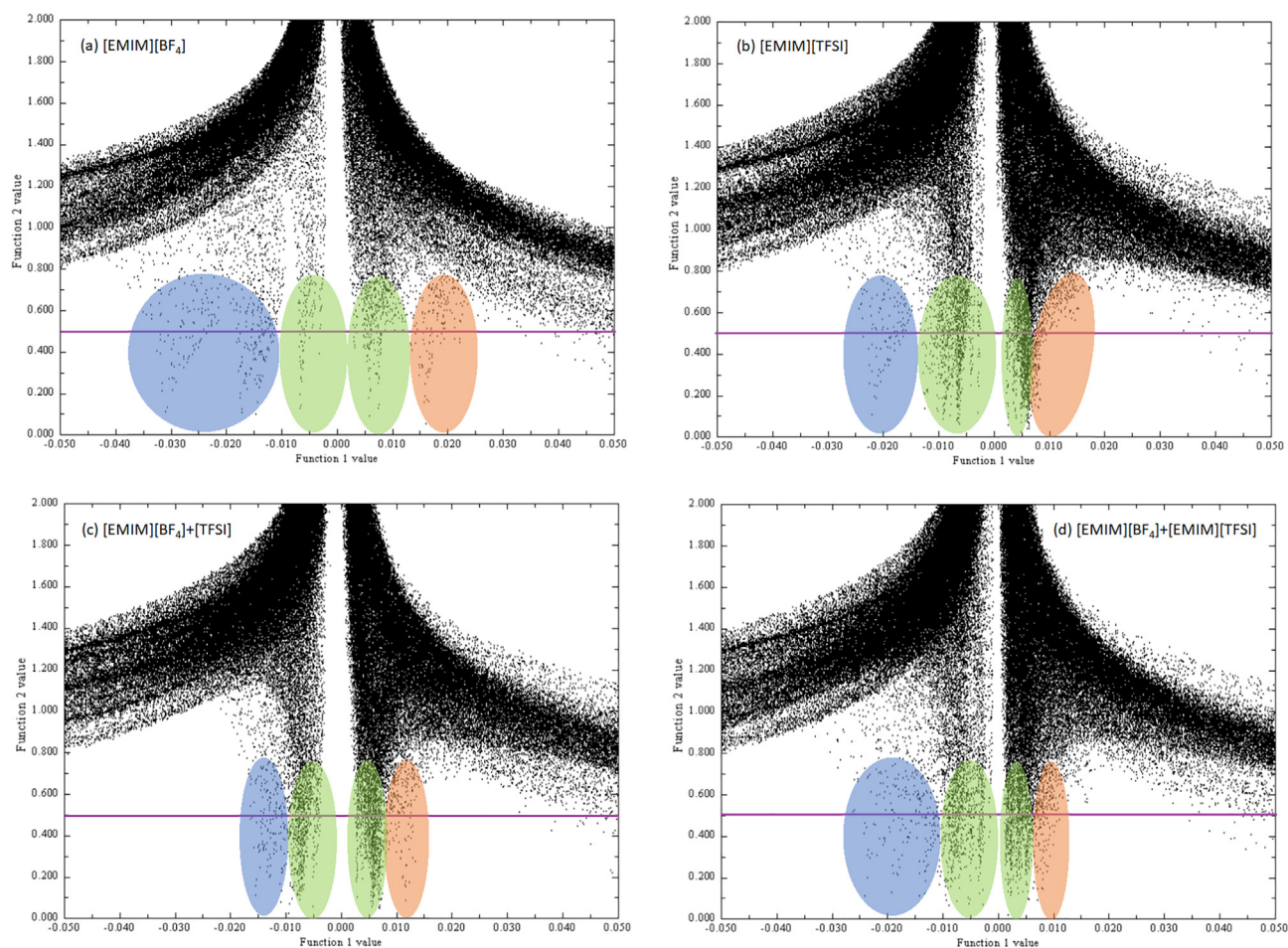


Fig. 9. Reduced density gradient (RDG) scatter plots (function 1 value is $\text{sign}(\lambda_2)\rho$ and function 2 value is RDG functions). Blue shaded area represents hydrogen bonding; green shaded area represents van der Waals interactions and red shaded area represent intra-molecular steric effects.

to van der Waals interactions instead to stronger hydrogen bonding. This mechanism is maintained for the considered dimers, trimer and tetramer.

The associated molecular orbitals for HOMO and LUMO are reported in Fig. 10 as well as the corresponding energy gap in Table 1. The values of energy gaps close to the spectral visible region for all the considered systems are a proof of the stability

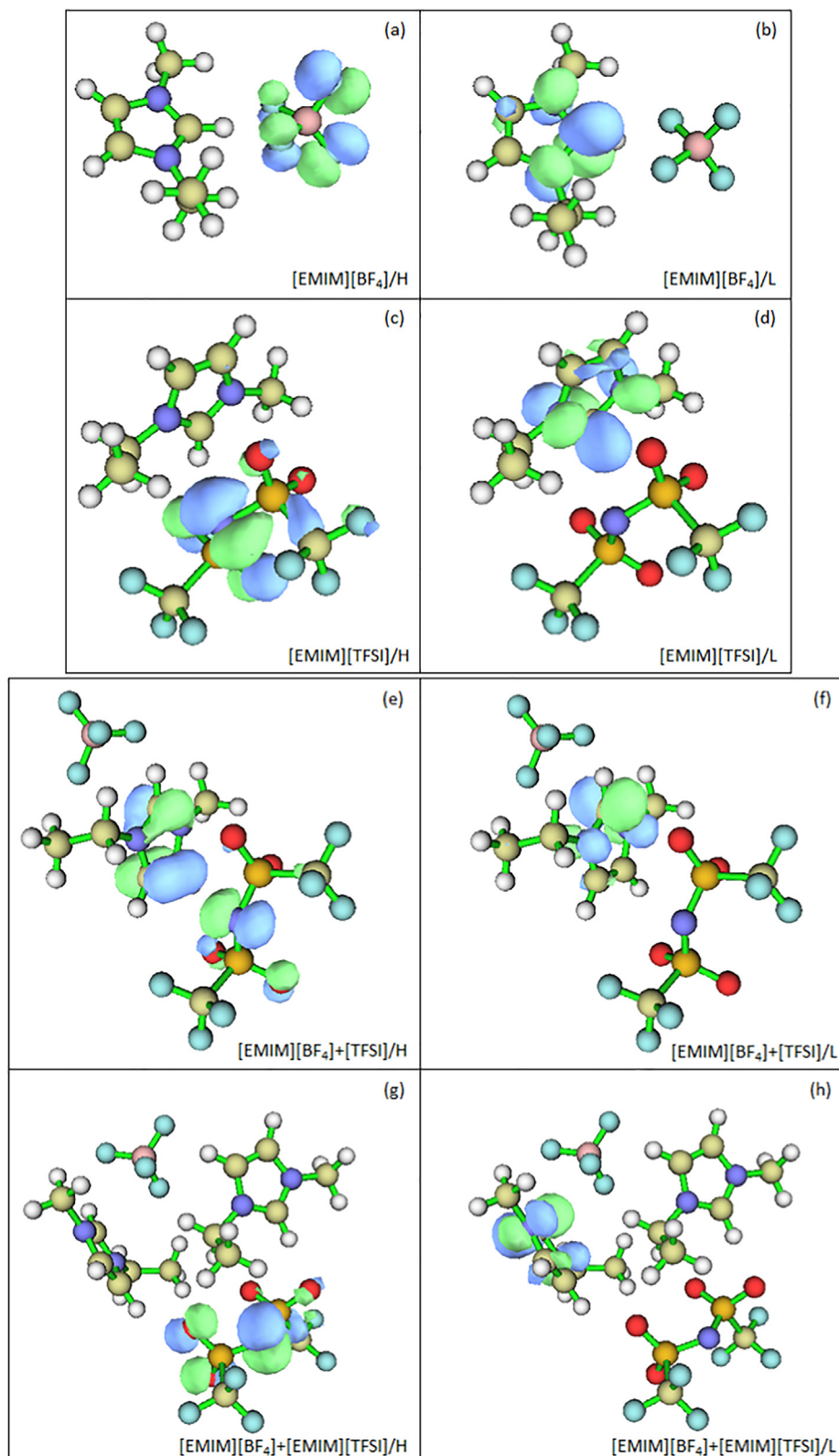


Fig. 10. The HOMO–LUMO graphs for each structure (showing positive (blue) and negative (green) isosurfaces) are embedded in the figures a-h.

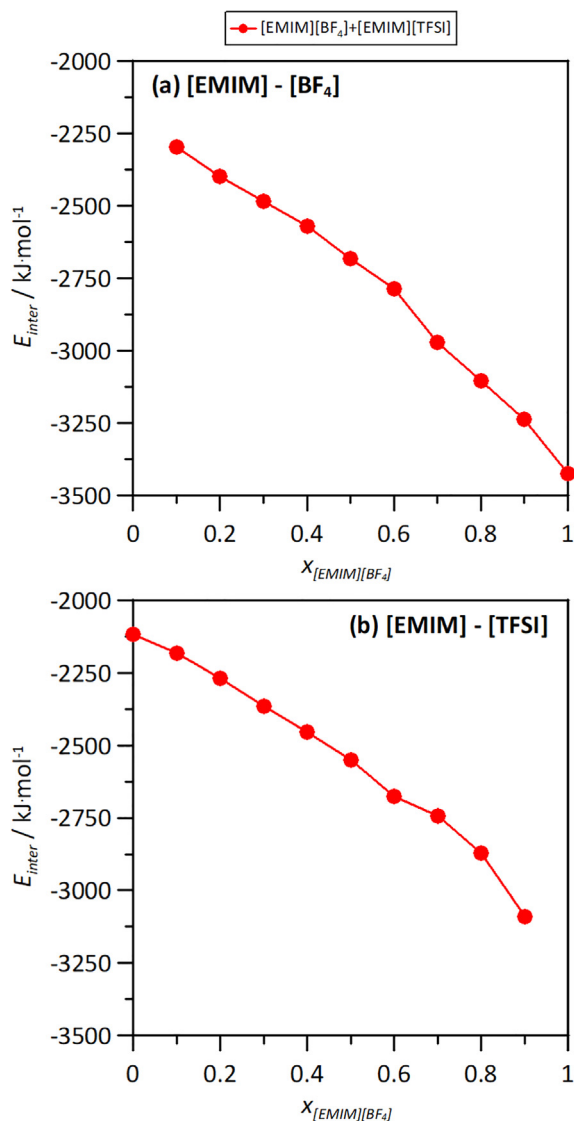


Fig. 11. Intermolecular interaction energy, E_{inter} (sum of Lennard-Jones and coulombic contributions), for the reported interacting pairs in x $[EMIM][BF_4]$ + $(1-x)$ $[EMIM][TFSI]$ mixtures at 298 K and 1 bar.

of the considered dimers, trimer and tetramer interactions in agreement with the large interaction energies reported in Table 1. The HOMO-LUMO energy gaps are practically the same for all the systems, thus showing similar mechanisms of interaction. Likewise, there is not a rule for the molecular location of the HOMO and LUMO orbitals, which can be located both in $[EMIM]^+$ cation or in the corresponding $[BF_4]^-$ or $[TFSI]^-$ anion, depending on the site of interaction.

3.3. MD study of $[EMIM][BF_4]$ + $[EMIM][TFSI]$ liquid structuring

Although DFT results allow a quantification of intermolecular interactions characteristics, only short range effects are considered. Interactions in liquid phases are characterized by longer effects which are theoretically analysed by using MD simulations. The considered force field as reported in Table S3 (Supplementary Information) was validated by the comparison of MD predicted density values and experimental data, Figure S4 (Supplementary Information). The experimental and theoretical values obtained are in suitable agreement, with largely non-ideal behaviour of mixture density predicted by MD. Therefore, we use this approach for inferring molecular level information on the intermolecular interactions and additional nanoscopic effects upon $[EMIM][BF_4]$ + $[EMIM][TFSI]$ mixing.

Anion-cation interactions at the microscopic level are firstly analysed by using intermolecular interaction energies, Fig. 11. E_{inter} provide a quantification of the strength of the different intermolecular interactions in the studied mixtures. Larger values for $[EMIM]-[BF_4]$ interactions are obtained, corresponding to strong electrostatic interactions. The composition evolution of cation-anion interactions energy, increasing (in absolute value) with increasing $[EMIM]-[BF_4]$ content, follows a non-linear pattern, with larger (absolute) values than the corresponding linear evolution with composition.

The structural properties of cation-anion interactions were also analysed using site-site radial distribution functions, RDFs, Fig. 12. It is well-known that prevailing interactions between $[EMIM]$ and $[BF_4]^-$ / $[TFSI]^-$ occur through the imidazolium CH(2) site (placed between the two N atoms in imidazolium ring) acting as donor [62,63] and the ability of $[BF_4]^-$ / $[TFSI]^-$ molecules for acting as acceptors (in the case of $[BF_4]^-$, through the F site, and in the case of $[TFSI]^-$, through the O site). $[EMIM]-[BF_4]$ interactions (hydrogen bonding) for the CH-F site show up to three interaction peaks, which are maintained in the whole composition range. The same

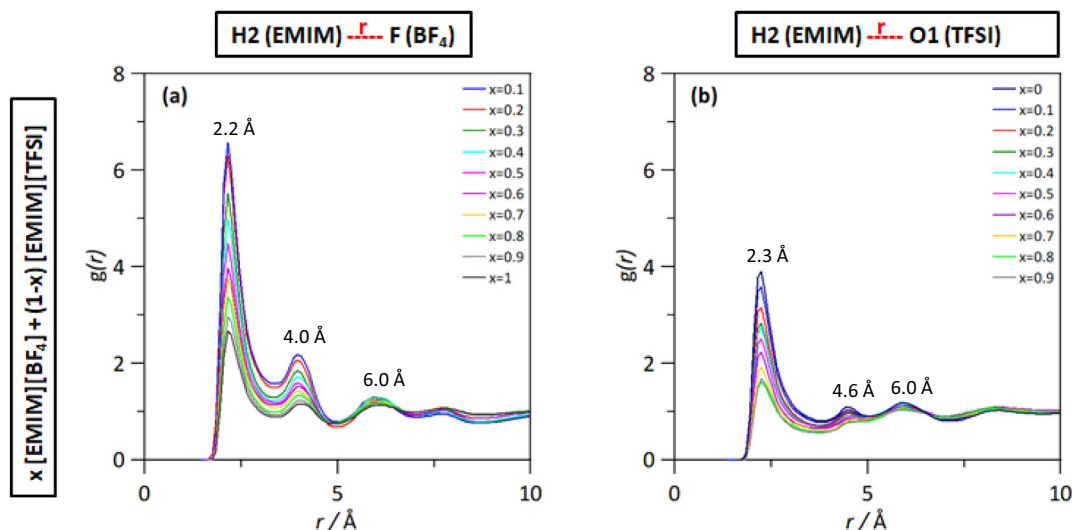


Fig. 12. Site-site radial distribution functions, $g(r)$, for the reported sites in x $[EMIM][BF_4]$ + $(1-x)$ $[EMIM][TFSI]$, x stands for mole fraction, at 298 K and 1 bar.

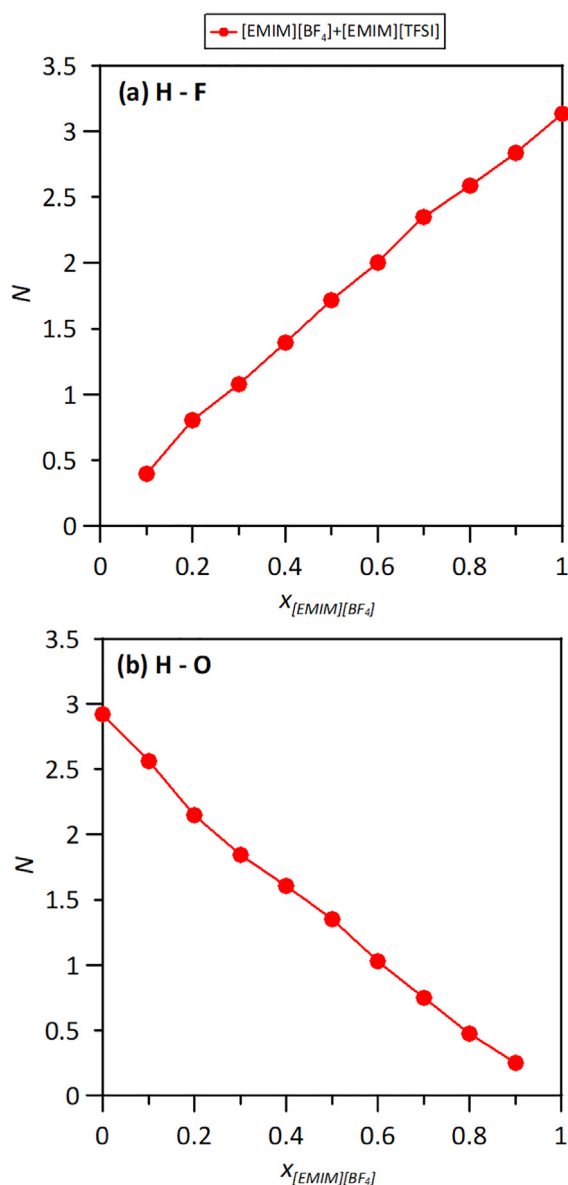


Fig. 13. Solvation numbers, N , obtained from the integration of radial distribution functions reported in Fig. 6, corresponding to the first solvation sphere, defined as the first minimum in the corresponding radial distribution function in \times [EMIM][BF₄] + (1- x) [EMIM][TFSI], x stands for mole fraction, at 298 K and 1 bar.

behaviour is observed for [EMIM]-[TFSI] interactions, confirming that hydrogen bonding is developed through the CH-O site. However, the [EMIM]-[TFSI] interactions lead to less intense peaks than [EMIM]-[BF₄] interactions, which is in accordance with the values of E_{inter} in Fig. 11 (weaker interactions with the [TFSI] anion, stronger interactions with the [BF₄] anion). The integration of RDFs to obtain solvation numbers, N , is reported in Fig. 13, i.e. the number of counterions in the first solvation sphere. In the case of H-F interaction (Fig. 13a), the composition evolution of N follows a non-linear evolution, with values larger than pure dilution effect (i.e. linear evolution), thus confirming the large aggregation trend of [BF₄] anion. In the case of H-O interaction (Fig. 13b), the results show that for [TFSI] rich solutions, many [TFSI] anions are hydrogen bonded to [EMIM], but when [EMIM]-[BF₄] content increases this hydrogen bonding decreases, because of the competing effect of [EMIM]-[BF₄] interactions, Fig. 13a, and thus for [EMIM]-[BF₄] rich mixtures, [TFSI] are less hydrogen bonded to the [EMIM] cation. These competing effects between anions are confirmed by the spatial distribution functions (SDFs) around [EMIM] cation reported in Fig. 14. For all the mixtures and compositions, high density spots of anions around the imidazolium ring are inferred (stronger around the CH site), thus confirming the development of hydrogen bonding through these sites in the whole composition range and both for [BF₄] and [TFSI] anions. Furthermore, [TFSI] anions are placed in closer regions to the CH imidazolium ring (and in minor extension around the other CH groups in the ring), and although showing less localized distributions, these molecules compete for the hydrogen bond donor sites in the [EMIM] cation.

The characteristics of cation-anion hydrogen bonding was also analysed in detail by the so-called combined distribution functions (CDFs, calculated using TRAVIS software[42]) including the corresponding distance and angles for the donor-acceptor sites. CDFs for cation-anion interaction through the CH-F and CH-O sites are reported in Fig. 15, two spots are clearly inferred corresponding to the two peak maxima in RDFs as reported in Fig. 12 (one spot for [EMIM]-[BF₄] interaction, first row, and one spot for [EMIM]-[TFSI] interaction, second row). For [EMIM]-[BF₄] interaction, we observe more intense spots corresponding to an interaction angle of roughly 160°, while for [EMIM]-[TFSI] interaction we observe weaker spots with an interaction angle of roughly 135°. These values, which are maintained in the whole composition range, confirm the hydrogen bonding nature of cation-anion interactions.

The dynamics of hydrogen bonding is analysed by the so-called residence times, t , Fig. 16. Larger t values were obtained for [TFSI] than for [BF₄], despite the stronger [EMIM]-[BF₄] than [EMIM]-[TFSI] interactions (Fig. 11). Therefore, [TFSI] anion has greater molecular mobility around [EMIM] cation than [BF₄] anion. Like-

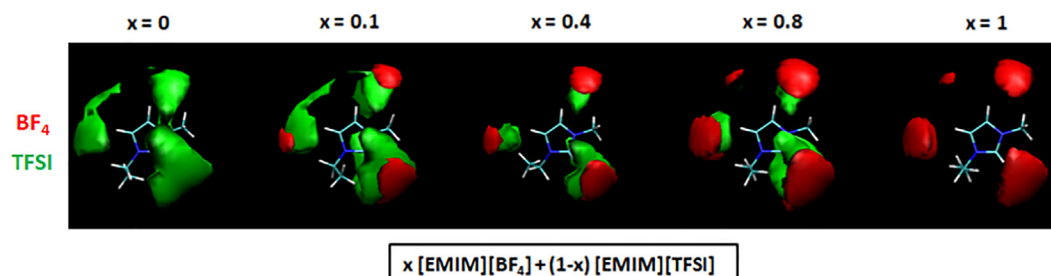


Fig. 14. Spatial distribution functions of the corresponding centers-of-mass around a central [EMIM][BF₄] ion for the reported mixtures at 298 K and 1 bar.

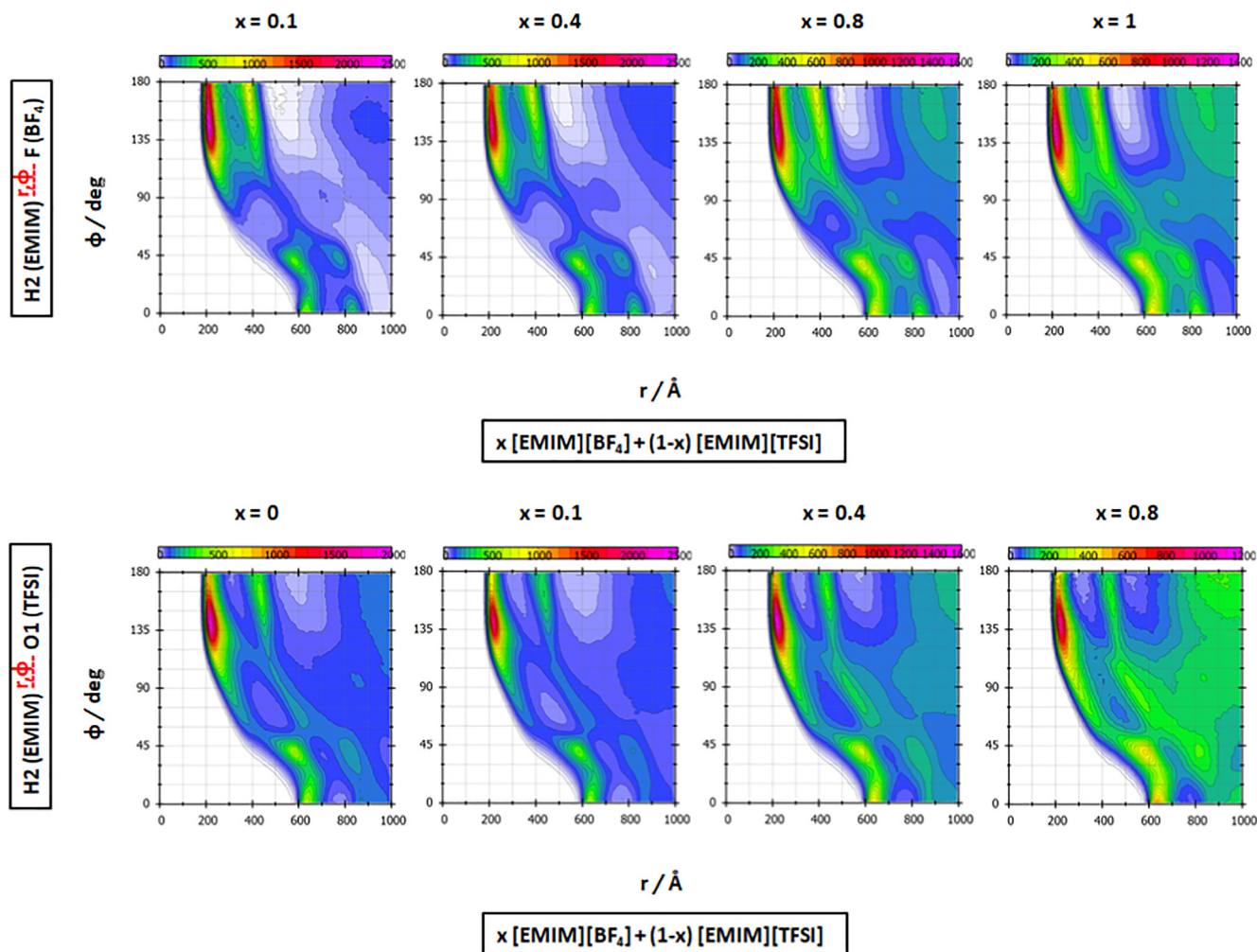


Fig. 15. Combined distribution functions of radial distribution functions (x-axis) and angular distribution functions (y-axis) for the reported distances, r , and angles, ϕ , (first row, [EMIM]-[BF₄] interactions; second row, [EMIM]-[TFSI] interactions) for x [EMIM][BF₄] + (1- x) [EMIM][TFSI] mixtures at 298 K and 1 bar.

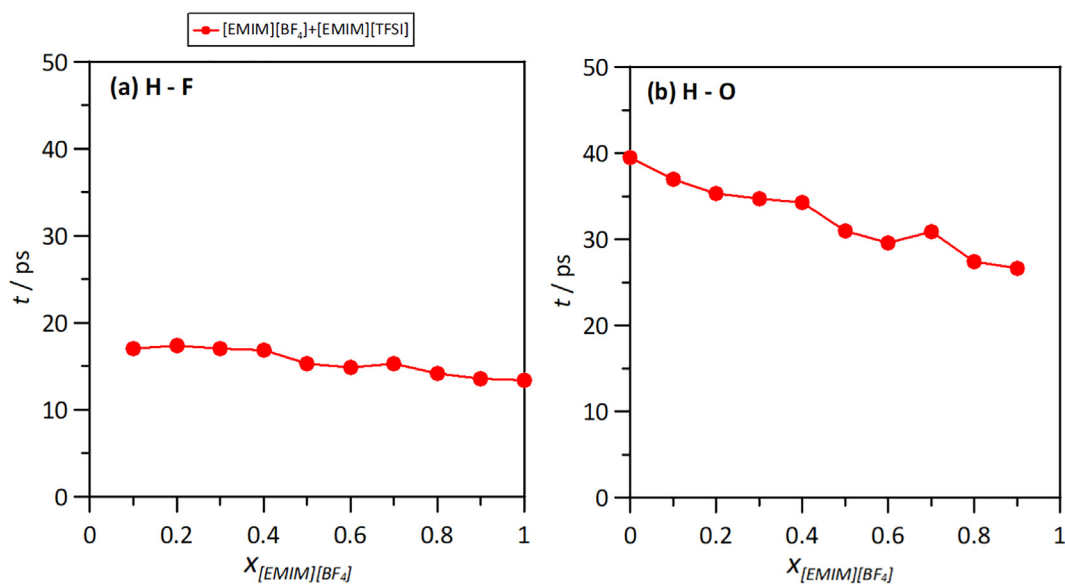


Fig. 16. Residence times, t , for selected atom pairs in x [EMIM][BF₄] + (1- x) [EMIM][TFSI] mixtures from MD simulations at 298 K and 1 bar. Residence times are calculated for first solvation layer defined according to the first minima in the corresponding $g(r)$.

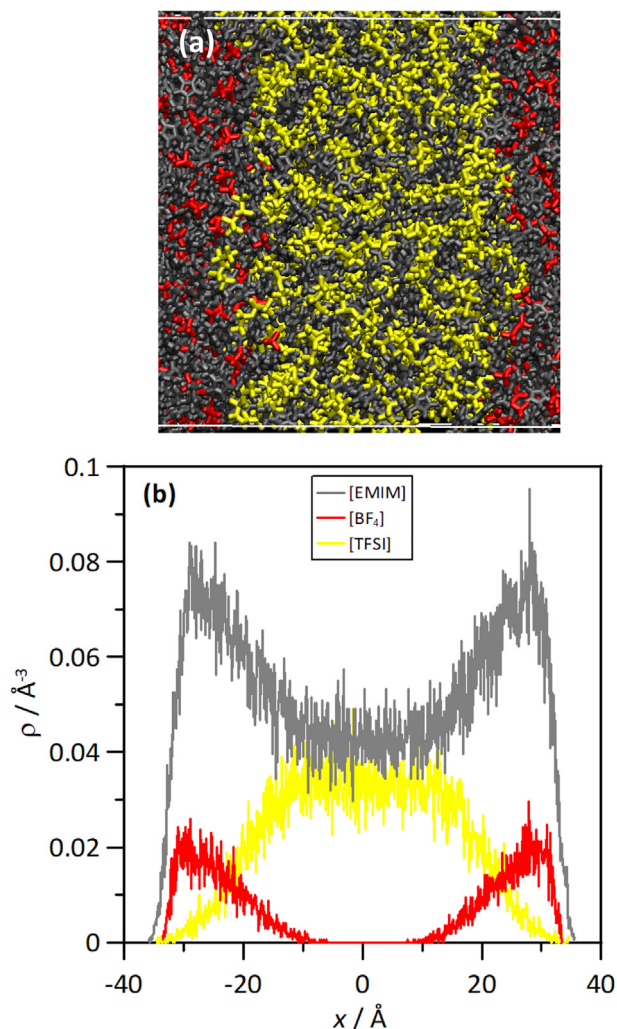


Fig. 17. (a) Snapshot and (b) number density profiles for x [EMIM][BF₄] + (1- x) [EMIM][TFSI] interface, $x = 0.5$. Values obtained from MD simulations at 298 K and 1 bar.

wise, in the case of [BF₄], the stronger [EMIM]-[BF₄] intermolecular interactions seem to control the dynamics of [EMIM] around [BF₄].

The main properties of [EMIM][BF₄] + [EMIM][TFSI] in liquid phase have been discussed in the previous paragraphs, but the properties of this double salt ionic liquid regarding to [EMIM][BF₄]-[EMIM][TFSI] interface (modelled as in Figure S2, Supplementary Information) were also analysed to infer the structural properties of [BF₄]⁻ and [TFSI]⁻ ions at the interface. The [EMIM][BF₄]-[EMIM][TFSI] interface is characterized by a strong adsorption of [BF₄]⁻ ions leading to a higher dense layer above [TFSI]⁻ ions, Fig. 17a. Regarding the structure of ions at the interface, results in Fig. 17b show that [BF₄]⁻ ions penetrate in [EMIM][TFSI] ionic liquid (i.e. starting diffusion toward bulk liquid phase for adsorption), which is showed by the widening of the density peaks.

4. Conclusions

The properties of [EMIM][BF₄] + [EMIM][TFSI] mixed ionic liquids were studied using a combined experimental and theoretical approach as a function of composition and temperature. The mixtures are characterized by a largely non-ideal behaviour which is related with the development of new intermolecular forces with changing anionic composition. The reported thermophysical prop-

erties, especially excess and mixing functions, confirm non-ideality for the studied systems. This non-ideality would require complex predictive models for the properties of mixed ionic liquids well beyond the linear mixing rules commonly proposed in the literature. This is even more remarkable for dynamic properties such as viscosity, for which an extremely complex behaviour with mixture composition is reported in his work. The reported molecular modelling studies allowed to quantify the nature, extension and strength of intermolecular forces, confirming the prevailing roles of hydrogen bonding, which determine the cation-anion interactions. These hydrogen bonds being different for the two considered anions are on the basis of the properties of the studied mixtures. Therefore, the considered mixed ILs, containing a common imidazolium cation and two different anion with variable concentration, are complex systems, whose properties cannot be explained with a simple anion replacement mechanism, which is on the roots of the largely non-ideal behaviour from the thermodynamic viewpoint. Thus, ILs containing several types of ions, anions in this work, can be considered for tuning ILs properties, increasing and changing the nature of these fluids, and thus the suitability for different applications. Nevertheless, the large non-ideality of these mixtures should be taken into account for predicting and designing their properties.

Declaration of Competing Interest

The authors declared that there is no conflict of interest.

Acknowledgements

This work was funded Ministerio de Ciencia, Innovación y Universidades (Spain, project RTI2018-101987-B-I00) and by Junta de Castilla y León (Spain, project BU094G18). We acknowledge SCAYLE (Supercomputación Castilla y León, Spain) for providing supercomputing facilities. The statements made herein are solely the responsibility of the authors. Authors declare no competing interests.

Appendix A. Supplementary data

Supplementary data to this article can be found online at <https://doi.org/10.1016/j.molliq.2021.116049>.

References

- [1] R. Ludwig, U. Kragl, Do we understand the volatility of ionic liquids?, *Angew. Chem. Int. Ed.* 46 (2007) 6582–6584.
- [2] B. Wang, L. Qin, T. Mu, Z. Xue, G. Gao, Are ionic liquids chemically stable?, *Chem. Rev.* 117 (2017) 7113–7131.
- [3] J.P. Hallett, T. Welton, Room-temperature ionic liquids: solvents for synthesis and catalysis, *Chem. Rev.* 111 (2011) 3508–3576.
- [4] C.J. Clarke, W.C. Tu, O. Levers, A. Brohl, J.P. Hallett, Green and sustainable solvents in chemical processes, *Chem. Rev.* 118 (2018) 747–800.
- [5] R.D. Rogers, Reflections on ionic liquids, *Nature* 447 (2007) 917–918.
- [6] X. Liu, Y. Huang, Y. Zhao, R. Gani, X. Zhang, S. Zhang, Ionic liquid design and process simulation for decarbonization of shale gas, *Ind. Eng. Chem. Res.* 55 (2016) 5931–5944.
- [7] G. Chatel, J.F.B. Pereira, V. Debbeti, H. Wang, R.D. Rogers, Mixing ionic liquids – “simple mixtures” or “double salts”?, *Green Chem.* 16 (2014) 2051–2083.
- [8] J.F.B. Pereira, P.S. Barber, S.P. Kelley, P. Benton, R.D. Rogers, Double salt ionic liquids based on 1-ethyl-3-methylimidazolium acetate and hydroxylfunctionalized ammonium acetates: strong effects of weak interactions, *PCCP* 19 (2017) 26934–26943.
- [9] R.P. Matthews, I.J. Villar-Garcia, C.C. Weber, J. Griffith, F. Cameron, J.P. Hallett, P.A. Hunt, T. Welton, A Structural Investigation of Ionic Liquid Mixtures, *PCCP* 18 (2016) 8608–8624.
- [10] H. Niedermeyer, J.P. Hallett, I.J. Villar-Garcia, P.A. Hunt, T. Welton, Mixtures of ionic liquids, *Chem. Soc. Rev.* 41 (2012) 7780–7802.
- [11] J.S.N. Canongia-lopes, T.C. Cordeiro, J.M.S.S. Esperanca, H.J.R. Guedes, S. Huq, L. P.N. Rebelo, K.R. Seddon, Deviations from ideality in mixtures of two ionic liquids containing a common ion, *J. Phys. Chem. B* 109 (2005) 3519–3525.

- [12] A. Stoppa, R. Buchner, G. Hefter, How ideal are binary mixtures of room-temperature ionic liquids?, *J. Mol. Liq.* 153 (2010) 46–51.
- [13] M. Larriba, P. Navarro, J. García, F. Rodríguez, Separation of toluene from n-heptane, 2,3-dimethylpentane, and cyclohexane using binary mixtures of [4empy][Tf2N] and [emim][DCA] ionic liquids as extraction solvents, *Sep. Purif. Technol.* 120 (2013) 392–401.
- [14] G. Annat, M. Forsyth, D.R. McFarlane, Ionic Liquid Mixtures—Variations in Physical Properties and Their Origins in Molecular Structure, *J. Phys. Chem. B* 116 (2012) 8251–8258.
- [15] P. Navia, J. Troncoso, L. Romani, Excess magnitudes for ionic liquid binary mixtures with a common ion, *J. Chem. Eng. Data* 52 (2007) 1369–1374.
- [16] P. Navia, J. Troncoso, L. Romani, Viscosities for ionic liquid binary mixtures with a common ion, *J. Sol. Chem.* 37 (2008) 677–688.
- [17] M.B. Oliveira, M. Dominguez-Perez, O. Cabeza, J.A. López-da-Silva, M.G. Freire, J.A.P. Coutinho, Surface tensions of binary mixtures of ionic liquids with bis (trifluoromethylsulfonyl)imide as the common anion, *J. Chem. Thermodyn.* 64 (2013) 22–27.
- [18] C. Moya, M. Gonzalez, F. Rodríguez, A. Soto, H. Rodríguez, J. Palomar, Non-ideal behavior of ionic liquid mixtures to enhance CO₂ capture, *Fluid Phase Equilib.* 450 (2017) 175–183.
- [19] P. Dhakal, J.K. Shah, Recent advances in molecular simulations of ionic liquid-ionic liquid mixtures, *Curr. Opin. Green Sus. Chem.* 18 (2019) 90–97.
- [20] B.S. Lee, S.T. Lin, Prediction and screening of solubility of pharmaceuticals in single- and mixed-ionic liquids using COSMO-SAC model, *AIChE J.* 63 (2017) 3096–3104.
- [21] A.M. Pinto, H. Rodríguez, Y.J. Colón, A. Arce, A. Arce Jr., A. Soto, Adsorption of carbon dioxide in two binary mixtures of ionic liquids, *Ind. Eng. Chem. Res.* 52 (2013) 5975–5984.
- [22] Z.G. Lei, J. Han, B. Zhang, Q. Li, J. Zhu, B. Chen, Solubility of CO₂ in binary mixtures of room-temperature ionic liquids at high pressures, *J. Chem. Eng. Data* 57 (2012) 2153–2159.
- [23] A.M. Smith, A.A. Lee, S. Perkin, Switching the structural force in ionic liquid solvent mixtures by varying composition, *Phys. Rev. Lett.* 118 (2017) 096002.
- [24] M. Chen, R. Pendrill, G. Widmalm, J.W. Brady, J. Wohlert, Molecular dynamics simulations of the ionic liquid 1-n-Butyl-3-Methylimidazolium chloride and its binary mixtures with ethanol, *J. Chem. Theory Comput.* 10 (2014) 4465–4479.
- [25] V.R. Ferro, C. Moya, D. Moreno, R. Santiago, J. de Riva, G. Pedrosa, M. Larriva, I. Diaz, J. Palomar, Enterprise ionic liquids database [ILUAM] for use in Aspen ONE programs suite with COSMO-based property methods, *Ind. Eng. Chem. Res.* 57 (2018) 980–989.
- [26] A. Gutiérrez, M. Atilhan, R. Alcalde, J.L. Trenzado, S. Aparicio, Insights on the mixtures of imidazolium based ionic liquids with molecular solvents, *J. Mol. Liq.* 255 (2018) 199–207.
- [27] R. Alcalde, M. Atilhan, S. Aparicio, Insights on 1-butyl-3-methylimidazolium bis (trifluoromethylsulfonyl) imide + ethanol liquid mixtures: a molecular dynamics approach, *J. Chem. Eng. Data* 61 (2016) 2729–2737.
- [28] C. Herrera, R. Alcalde, M. Atilhan, S. Aparicio, Microscopic characterization of mixtures of amino acid ionic liquids and organic solvents, *J. Mol. Liq.* 250 (2019) 111–120.
- [29] J.L. Trenzado, R. Alcalde, M. Atilhan, S. Aparicio, Molecular dynamics and experimental characterization of [BMIM][BF₄] and [BMIM][PF₆] with ether cosolvent binary mixtures, *J. Mol. Liq.* 271 (2018) 65–73.
- [30] J.L. Trenzado, A. Gutiérrez, R. Alcalde, M. Atilhan, S. Aparicio, Insights on [BMIM][BF₄] and [BMIM][PF₆] ionic liquids and their binary mixtures with acetone and acetonitrile, *J. Mol. Liq.* 294 (2019) 111632.
- [31] S. Aparicio, M. Atilhan, F. Karadas, Thermophysical properties of pure ionic liquids: review of present situation, *Ind. Eng. Chem. Res.* 49 (2010) 9580–9595.
- [32] X. Wang, Y. Chi, T. Mu, A review on the transport properties of ionic liquids, *J. Mol. Liq.* 193 (2014) 262–266.
- [33] W. Wagner, A. Pru, The IAPWS Formulation 1995 for the Thermodynamic Properties of Ordinary Water Substance for General and Scientific Use, *J. Phys. Chem. Ref. Data* 31 (2002) 1995 387–535.
- [34] E. W. Lemmon, M. L. Huber, M. McLinden, Reference Fluid, Thermodynamic, Transport Properties. NIST Standard Reference Database 23, version 9.0; The National Institute of Standards, Technology: Gaithersburg, MD, 2010.
- [35] M.M. Alavianmehr, R. Ahmadi, N. Aguilar, M. El-Shaik, S.M. Hosseini, S. Aparicio, Thermophysical and molecular modelling insights into glycerol + alcohol liquid mixtures, *J. Mol. Liq.* 297 (2020) 111811.
- [36] S. Adams, P. de Castro, P. Echenique, J. Estrada, M.D. Hanwell, P. Murray-Rust, P. Sherwood, J. Thomas, J.A. Townsend, The Quixote project: collaborative and open quantum chemistry data management in the internet age, *J. Cheminformatics* 3 (2011) 38.
- [37] F. Neese, The ORCA program system, *WIREs Comput. Mol. Sci.* 2 (2012) 73–78.
- [38] C. Lee, W. Yang, R.G. Parr, Development of the Colle-salvetti correlation-energy formula into a functional of the electron density, *Phys. Rev. B* 37 (1988) 785–789.
- [39] A.D. Becke, Density-functional exchange-energy approximation with correct asymptotic behavior, *Phys. Rev. A* 38 (1988) 3098–3100.
- [40] S. Grimme, J. Antony, S. Ehrlich, H.A. Krieg, Consistent and accurate ab initio parametrization of density functional dispersion correction (DFT-D) for the 94 elements H–Pu, *J. Chem. Phys.* 132 (2010) 154104.
- [41] S. Simon, M. Duran, J.J. Dannenberg, How does basis set superposition error change the potential surfaces for hydrogen-bonded dimers?, *J. Chem. Phys.* 105 (1996) 11024–11031.
- [42] R.F.W. Bader, *Atoms in Molecules: a Quantum Theory*, Oxford University Press, 1990.
- [43] T. Lu, F. Chen, Multiwfn: A multifunctional wavefunction analyzer, *J. Comput. Chem.* 33 (2012) 580–592.
- [44] S. Aparicio, C.T. Yavuz, M. Atilhan, Molecular insights into benzimidazole-linked polymer interactions with carbon dioxide and nitrogen, *ChemistrySelect* 3 (2018) 3691–3701.
- [45] J. Xiao, Y.P. Zhao, X. Fan, J.P. Cao, G.J. Kang, W. Zhao, X.Y. Wei, hydrogen bonding interactions between the organic oxygen/nitrogen monomers of lignite and water molecules: A DFT and AIM study, *Fuel Process. Technol.* 168 (2017) 58–64.
- [46] V. Anbu, K.A. Vijayalakshmi, R. Karunathan, A.D. Stephen, P.V. Nidhin, Explosives properties of high energetic trinitrophenyl nitramide molecules: A DFT and AIM analysis, *Arab. J. Chem.* 12 (2019) 621–632.
- [47] E.R. Johnson, S. Keinan, P. Mori-Sanchez, J. Contreras-García, A.J. Cohen, W. Yang, Revealing non-covalent interactions, *J. Am. Chem. Soc.* 132 (2010) 6498–6506.
- [48] A.P. Lyubartsev, A. Laaksonen, MDynaMix - a scalable portable parallel MD simulation package for arbitrary molecular mixtures, *Comput. Phys. Commun.* 128 (2000) 565–589.
- [49] V. Zoete, M.A. Cuendet, A. Grosdidier, O. Michielin, SwissParam, A fast force field generation tool for small organic molecules, *J. Comput. Chem.* 32 (2011) 2359–2368.
- [50] T.A. Halgren, Merck molecular force field. I. Basis, form, scope, parameterization, and performance of MMFF94, *J. Comput. Chem.* 17 (1996) 490–519.
- [51] C.M. Breneman, K.B. Wiberg, Determining atom-centered monopoles from molecular electrostatic potentials. The need for high sampling density in formamide conformational analysis, *J. Comput. Chem.* 11 (1990) 361–373.
- [52] L. Martínez, R. Andrade, E.G. Birgin, J.M. Martínez, Packmol: A package for building initial configurations for molecular dynamics simulations, *J. Comput. Chem.* 30 (2009) 2157–2164.
- [53] U.L. Essmann, M.L.; Perera, T. Berkowitz, H. Darden, H. Lee, L.G. Pedersen, A smooth particle mesh Ewald method, *J. Chem. Phys.* 103 (1995) 8577–8593.
- [54] M. Tuckerman, B.J. Berne, G.J. Martyna, Reversible multiple time scale molecular dynamics, *J. Chem. Phys.* 97 (1992) 1990–2001.
- [55] W. Humphrey, A. Dalke, K. Schulten, VMD - Visual molecular dynamics, *J. Molec. Graphics* 14 (1996) 33–38.
- [56] M. Brehm, B. Kirchner, TRAVIS - A free analyzer and visualizer for Monte Carlo and molecular dynamics trajectories, *J. Chem. Inf. Model.* 51 (2011) 2007–2023.
- [57] H. Shekaari, M.T. Zafarani-Moattar, M. Mokhtarpour, S. Faraji, Volumetric and compressibility properties for aqueous solutions of choline chloride based deep eutectic solvents and Prigogine-Flory-Patterson theory to correlate of excess molar volumes at T = (293.15 to 308.15) K, *J. Mol. Liq.* 289 (2019) 111077.
- [58] K. Dong, S. Zhang, D. Wang, X. Yao, Hydrogen bonds in imidazolium ionic liquid mixtures, *J. Phys. Chem. A* 110 (2006) 9775–9782.
- [59] M.Z. Brela, P. Kubisiak, A. Eilmes, Understanding the structure of the hydrogen bond network and its influence on vibrational spectra in a prototypical aprotic ionic liquid, *J. Phys. Chem. B* 122 (2018) 9527–9537.
- [60] H. Roohi, A.R. Nowroozi, E. Anjomshoa, H-bonded complexes of uracil with parent nitrosamine: a quantum chemical study, *Comput. Theor. Chem.* 965 (2011) 211–220.
- [61] E.R. Johnson, S. Keinan, P. Mori-Sanchez, J. Contreras-García, A.J. Cohen, W. Yang, Revealing noncovalent interactions, *J. Am. Chem. Soc.* 132 (2010) 6498–6506.
- [62] K. Dong, S. Zhang, D. Wang, X. Yao, Hydrogen bonds in imidazolium ionic liquids, *J. Phys. Chem. A* 110 (2006) 9775–9782.
- [63] K. Dong, S. Zhang, J. Wang, Understanding the hydrogen bonds in ionic liquids and their roles in properties and reactions, *Chem. Comm.* 52 (2016) 6744–6764.